Since January 2020 Elsevier has created a COVID-19 resource centre with free information in English and Mandarin on the novel coronavirus COVID-19. The COVID-19 resource centre is hosted on Elsevier Connect, the company's public news and information website.

Journal of Molecular Graphics and Modelling 102 (2021) 107778

Contents lists available at ScienceDirect

Journal of Molecular Graphics and Modelling

journal homepage: www.elsevier.com/locate/JMGM

Exploring the intrinsic dynamics of SARS-CoV-2, SARS-CoV and MERS-CoV spike glycoprotein through normal mode analysis using anisotropic network model

Satyabrata Majumder, Dwaipayan Chaudhuri, Joyeeta Datta, Kalyan Giri*

Department of Life Sciences, Presidency University, Kolkata, India

ARTICLE INFO

Article history:
Received 5 August 2020
Received in revised form
5 October 2020
Accepted 13 October 2020
Available online 16 October 2020

Keywords:
SARS-CoV-2
SARS-CoV
MERS-CoV
Spike glycoprotein
Normal mode analysis

ABSTRACT

COVID-19 caused by SARS-CoV-2 have become a global pandemic with serious rate of fatalities. SARS-CoV and MERS-CoV have also caused serious outbreak previously but the intensity was much lower than the ongoing SARS-CoV-2. The main infectivity factor of all the three viruses is the spike glycoprotein. In this study we have examined the intrinsic dynamics of the prefusion, lying state of trimeric S protein of these viruses through Normal Mode Analysis using Anisotropic Network Model. The dynamic modes of the S proteins of the aforementioned viruses were compared by root mean square inner product (RMSIP), spectral overlap and cosine correlation matrix. S proteins show homogenous correlated or anticorrelated motions among their domains but direction of C_α atom among the spike proteins show less similarity. SARS-CoV-2 spike shows high vertically upward motion of the receptor binding motif implying its propensity for binding with the receptor even in the lying state. MERS-CoV spike shows unique dynamical motion compared to the other two S protein indicated by low RMSIP, spectral overlap and cosine correlation value. This study will guide in developing common potential inhibitor molecules against closed state of spike protein of these viruses to prevent conformational switching from lying to standing state.

1. Introduction

Coronaviruses are zoonotic pathogens which belong to the largest group of *Nidovirales* order [1] and has been shown to infect many avian and mammalian species [2]. Severe acute respiratory syndrome coronavirus (SARS-CoV), Middle East respiratory syndrome coronavirus (MERS-CoV) and novel coronavirus (SARS-CoV-2) are in betacoronavirus family but with different lineages. SARS-CoV-2, SARS-CoV belongs to lineage B whereas MERS-CoV belongs to lineage C but a common factor is that they all cause acute lung injury (ALI) and acute respiratory distress syndrome (ARDS) which leads to pulmonary failure and result in fatality. COVID-19 caused by novel coronavirus (SARS-CoV-2), has now emerged as global pandemic and high rate of fatalities have been reported globally [3–5]. The major surface protein of all these 3 coronaviruses is called spike glycoprotein (S) which is responsible for host attachment of the virus and entry into cell by membrane fusion. The protein protrudes out of the surface and is found in a trimeric configuration [6]. The protein has 2 subunits called S1 and S2. S1 subunit has the receptor binding domains (RBD) which help to stabilize the prefusion state. The S2 subunit remains anchored to the membrane and contains the fusion machinery and further cleaved to form S2' in certain coronaviruses thus activating the membrane fusion cascade [7,8]. The receptors recognized by the viruses are also different in case of MERS-CoV it is 5-N-acetyl-9-O-acetyl-sialosides found on glycoproteins and glyco-lipids at the host cell surface while for SARS-CoV and SARS-CoV-2 it is hACE2 receptor [9,10]. Spike glycoprotein undergoes conformational switch in order to bind with the receptor. In lying or closed state the receptor binding domain is buried deeply into the trimer core and so it is not accessible to the receptor making the conformational switch essential. In standing or open state one of the RBD protrudes out of the trimer core and becomes accessible to the receptor [11]. A detailed study to explore the intrinsic dynamical motion of the prefusion lying state spike protein trimer is needed for proper understanding of its function from conformation perspective.

In recent years characterization of whole protein collective and

* Corresponding author. Department of Life Sciences, Presidency University, 86/1 College Street, Kolkata, 700073, India.
E-mail address: kalyan.dbs@presiuniv.ac.in (K. Giri).

https://doi.org/10.1016/j.jmgm.2020.107778
1093-3263/

domain-specific motions have been accomplished using normal mode calculations [12,13]. Coarse-grained normal mode analysis (CG-NMA) has now become a valuable tool for studying the biologically relevant conformational motions of large protein or protein complex. Although coarse-grained NMA (CG-NMA) does not capture the detailed local dynamics that are obtained from all atom molecular dynamics simulation, CG-NMA has been shown to be equally effective in demonstrating the global functional motions of proteins [14,15]. NMA with anisotropic network model (ANM), a variant of elastic network model (ENM), has been proved to be successful in describing the collective dynamics of a wide range of biomolecular systems [16–18]. Notable application of NMA using ANM especially in membrane proteins has been thoroughly mentioned in the study and review done by Bahar et al. [19,20].

In this study we have explored the intrinsic dynamics of the closed or lying state spike (S) glycoprotein of SARS-CoV-2, SARS-CoV and MERS-CoV through NMA studies using ANM. We found noticeable variations in the dynamics of the proteins in different low frequency modes in terms of both magnitude and direction of displacement vectors. We found that receptor binding motif (RBM) of a single chain of SARS-CoV-2 spike show high fluctuation in the lying state indicating its high probability to bind with the receptor implying the high infectivity of SARS-CoV-2 than other two viruses. MERS-CoV S shows distinct dynamics than SARS-CoV S and SARS-CoV-2 S indicates its low sequence similarity and distant phylogenetic relationship with other. Detailed domain-wise motion, atomic fluctuation data and quantitative comparison between S protein structures of the mentioned viruses will aid in identifying common potential drug binding hotspots in the receptor binding domain of the protein which will guide in designing common inhibitor or modified version of these molecules through structure-based approach.

2. Materials and methods

2.1. Protein structure retrieval

All the X-ray crystal structures for SARS-CoV-2, SARS-CoV and MERS-CoV S proteins in the lying state were taken from protein data bank [21]. The corresponding PDB IDs are 6VXX, 5X58 and 6Q05 respectively [11,22,23]. CHARM-GUI was used to prepare the protein (i.e adding missing atoms and assigning correct protonation states) [24]. As a large part of this study is involved in the comparative analysis purposes, we have discarded part of the S2 region of S protein of all viral strains so that each protein model has equal number of Cα atoms (1087 in all three chains). S2 region of the protein does not take active part in receptor interaction.

2.2. Normal mode analysis (NMA) using anisotropic network model (ANM)

Detailed mathematical description about normal mode analysis and how it is applicable to protein molecule is given in many studies [20,25–27]. NMA is a technique to study vibrational motion of harmonic oscillating system near the equilibrium state. The motions are of small amplitude in a potential well and cannot cross energy barriers. At a minimum state q_0, the potential energy V can be obtained from the approximation of Taylor series expansion. For the generalized coordinates q_i:

$$V = \frac{1}{2}\left(\frac{\partial^2 V}{\partial q_i \partial q_j}\right)_0 \eta_i \eta_j = \frac{1}{2} V_{ij} \eta_i \eta_j \tag{1}$$

Where η_i specifies the deviation from equilibrium ($q_i = q_{0i} + \eta_i$). The kinetic energy T also approximated from Taylor expansion. The resulting Lagrangian is L = *T-V*, which results in linear differential equations of motion:

$$T_i \ddot{\eta}_i + V_{ij} \eta_j = 0 \tag{2}$$

Assuming oscillatory solution, $\eta_i = a_{ik}\cos(\omega_k t + \delta_k)$ and substituting it in Eq. (2) results in eigenvalue problem:

$$\boldsymbol{A}^T \boldsymbol{V} \boldsymbol{A} = \lambda \tag{3}$$

$\boldsymbol{A}$ is the matrix of amplitudes a_{ik}, and $\boldsymbol{V}$ is the matrix of the second derivative of the potential energy and is referred to as Hessian. λ is a diagonal matrix of eigenvalues. The pattern of motions is fully specified by the vibrational normal modes, i.e. the eigenvectors (A_k) and their associated eigenvalues (λ_k). The vector describes the directionality and magnitude of motion of each particle relative to other particles.

Anisotropic network model (ANM) is best described in the paper authored by Bahar et al. [19]. It is a variant of Elastic network model (ENM) where nodes are identified by the positions of Cα atoms and an uniform spring constant γ (in this study we have taken $\gamma = 15$) is adopted for the bonds. Then the potential is calculated by the following expression:

$$V = \frac{\gamma}{2\sum_{j|j\neq i}(\boldsymbol{\Gamma}_{ij})\left(R_{ij} - R_{ij}^0\right)^2} \tag{4}$$

Here R_{ij} and R_{ij}^0 are instantaneous and equilibrium distances between the nodes i and j, $\boldsymbol{\Gamma}_{ij}$ is the ij th element of the Kirchhoff matrix $\boldsymbol{\Gamma}$ of inter-residue contacts, equal to 1 if nodes i and j are within an interaction cutoff distance r_c, zero otherwise. Resulting Hessian matrix $\boldsymbol{H}$ for a network of N nodes is a 3 N × 3 N matrix composed of N x N super elements, $\boldsymbol{H}_{ij}$:

$$\boldsymbol{H}_{ij} = \frac{\gamma \Gamma_{ij}}{\left(R_{ij}^0\right)^2}\begin{bmatrix} X_{ij}X_{ij} & X_{ij}Y_{ij} & X_{ij}Z_{ij} \\ Y_{ij}X_{ij} & Y_{ij}Y_{ij} & Y_{ij}Z_{ij} \\ Z_{ij}X_{ij} & Z_{ij}Y_{ij} & Z_{ij}Z_{ij} \end{bmatrix} \tag{5}$$

Here X_{ij}, Y_{ij} and Z_{ij} are the components of the distance vector R_{ij}^0. The resulting eigenvalue equation looks in the form:

$$\boldsymbol{H}^{-1} = \sum_{i=1}^{3N-6} \frac{1}{\lambda_i} \boldsymbol{u}_i \boldsymbol{u}_i^T \tag{6}$$

Here we consider (3 N - 6) non zero modes, λ_i corresponds to eigenvalues and the corresponding eigenvectors are $\boldsymbol{u}_i$. The inverse $\boldsymbol{H}^{-1}$ is also organized in N x N submatrices of size 3 × 3, each. The ij th submatrix H_{ij}^{-1} defines the covariance between the fluctuations of residues i and j. The cross-correlation (CC) between the equilibrium fluctuations of residues i and j, $\Delta\boldsymbol{R}_i \cdot \Delta\boldsymbol{R}_j$ is expressed in terms of the trace (tr) of these submatrices as:

$$C_{ij} \equiv \langle \Delta\boldsymbol{R}_i \cdot \Delta\boldsymbol{R}_j \rangle = \frac{\mathrm{tr}\left(\boldsymbol{H}_{ij}^{-1}\right)}{\sqrt{\mathrm{tr}\left(\boldsymbol{H}_{ii}^{-1}\right)\mathrm{tr}\left(\boldsymbol{H}_{ij}^{-1}\right)}} \tag{7}$$

We have performed the NMA and all the analysis functions including root mean squared inner product (RMSIP) [28], spectral overlap [29] and cosine correlation or overlap [30] using *ProDy* python package [31]. RMSIP computes quantitative comparison value between the sets of normal modes and expressed as:

$$\text{RMSIP} = \left(\frac{1}{10} \left[\sum_{i=1}^{10} \sum_{j=1}^{10} (X_i \cdot Y_j)^2 \right] \right)^{\frac{1}{2}} \quad (8)$$

Where $\boldsymbol{X_i}$ and $\boldsymbol{Y_j}$ represents the eigenvectors of a pair of proteins being compared and i and j represent the mode numbers.

Cosine correlation or overlap measures the similarity between two vectors of an inner product space. It is calculated by the cosine of the angle between the two vectors and determines whether two vectors are pointing roughly in same direction. The following mathematical formula is:

$$\cos\theta = \frac{\vec{a} \cdot \vec{b}}{\| \vec{a} \| \| \vec{b} \|} = \frac{\sum_1^n a_i b_i}{\sqrt{\sum_1^n a_i^2} \sqrt{\sum_1^n b_i^2}} \quad (9)$$

Where $\vec{a} \cdot \vec{b} = \sum_1^n a_i\, b_i = a_1 b_1 + a_2 b_2 + \cdots + a_n b_n$ is the dot product of two vectors. Its value ranges from 0 to 1 with 1 corresponds to 100% similar. We have also used in-house python scripts for the plotting purposes. Spectral overlap calculates overlap between covariances of modes 1 and modes 2, hence the dimension of the covariance matrix should be same in two comparing structures.VMD 1.9.2 was used for mode visualization and image rendering. Structural alignments of the models were done using PyMol.

3. Results

3.1. Characterization of normal modes of SARS-CoV-2, SARS-CoV and MERS-CoV spike glycoprotein (S protein)

We have computed the eigenvalues of first hundred non-zero normal modes of the SARS-CoV-2, SARS-CoV, and MERS-CoV spike (S) proteins in the lying state (Fig. 1). The energy associated with a given normal mode is directly proportional to its eigenvalue [28]. We have discarded the first six zero-eigenvalues, as those values correspond to the rigid motions (three translational and three rotational motions). Despite having similar kind of three-dimensional architecture, frequency of the normal modes do not overlap and significant variations are seen quite clearly in the lower as well as higher normal mode indices in the three S protein models. The spectra of the eigenvalues for the SARS-CoV-2 S is lower compared to the SARS-CoV S and MERS-CoV S, which indicates comparatively more collective motion in the former model. SARS-CoV S and MERS-CoV S show some overlaps in the mode indices 7–12 which may be considered as superficial.

3.2. Correlated dynamics of SARS-CoV-2, SARS-CoV and MERS-CoV spike (S) protein and visual analysis of the first four non-zero modes

We have assessed the extent to which the trimer conformation influences the dynamics of each S protein chain (Fig. 3). Overall the pattern of the cross correlation matrix (CCM) looks similar for three models and have similar domain wise correlated movement but the magnitude of correlation coefficients (CC) are different to some extent. According to PDB and Uniprot protein feature view, the position of S1 NTD, S1 CTD and RBD for the protein models are as follows: SARS-CoV: 14–290 is S1 NTD (N-terminal domain), 321–513 is S1 CTD (C terminal domain), 306–527 is RBD (binding motif is 424–494); SARS-CoV-2: 13–303 is S1 NTD, 334–527 is S1 CTD, 319–541 is RBD (binding motif is 437–508); MERS-CoV: 18–350 is S1 NTD, 381–588 is S1 CTD, 382–503 is RBD [11]. In Fig. 2, different functionally important domains of the three spike proteins are shown.

Multiple sequence alignment of the proteins is given in supplementary. Emphasizing the motions among the domains, it was found that SARS-CoV and SARS-CoV-2 S proteins have homogenous correlated displacements. S1 CTD and NTD of each chain have weak negative correlation with each other (−0.1 to −0.4). S1 CTD of one chain has weak negative correlation with CTD of other chains and same scenario is seen with the NTD. S1 CTD and NTD in each chain are negatively correlated with each other implying the RBM tries to move further from NTD in order to be accessible by the receptor. One of the interesting facts is that S1 NTD of one chain shows strong positive correlation with CTD of at least one of the two other

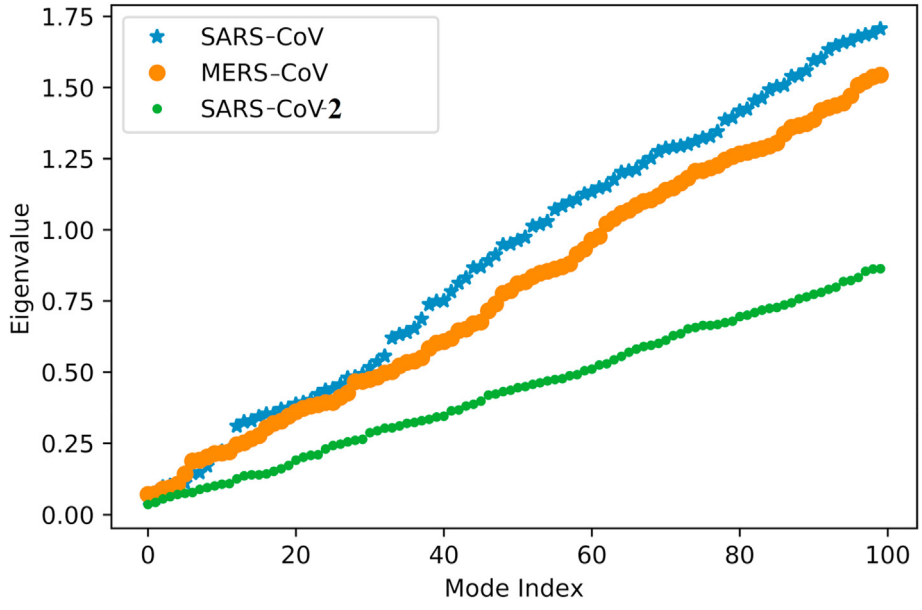

Fig. 1. The eigenvalues of first 106 normal modes of prefusion state of the S proteins of SARS-CoV, MERS-CoV, and SARS-CoV-2 are plotted against the normal mode index. The values are in arbitrary units as the spring constant is also in arbitrary unit. The first six zero-eigenvalue modes are not shown; so mode index 0 in this graph is equal to 7 and 100 is equal to 107.

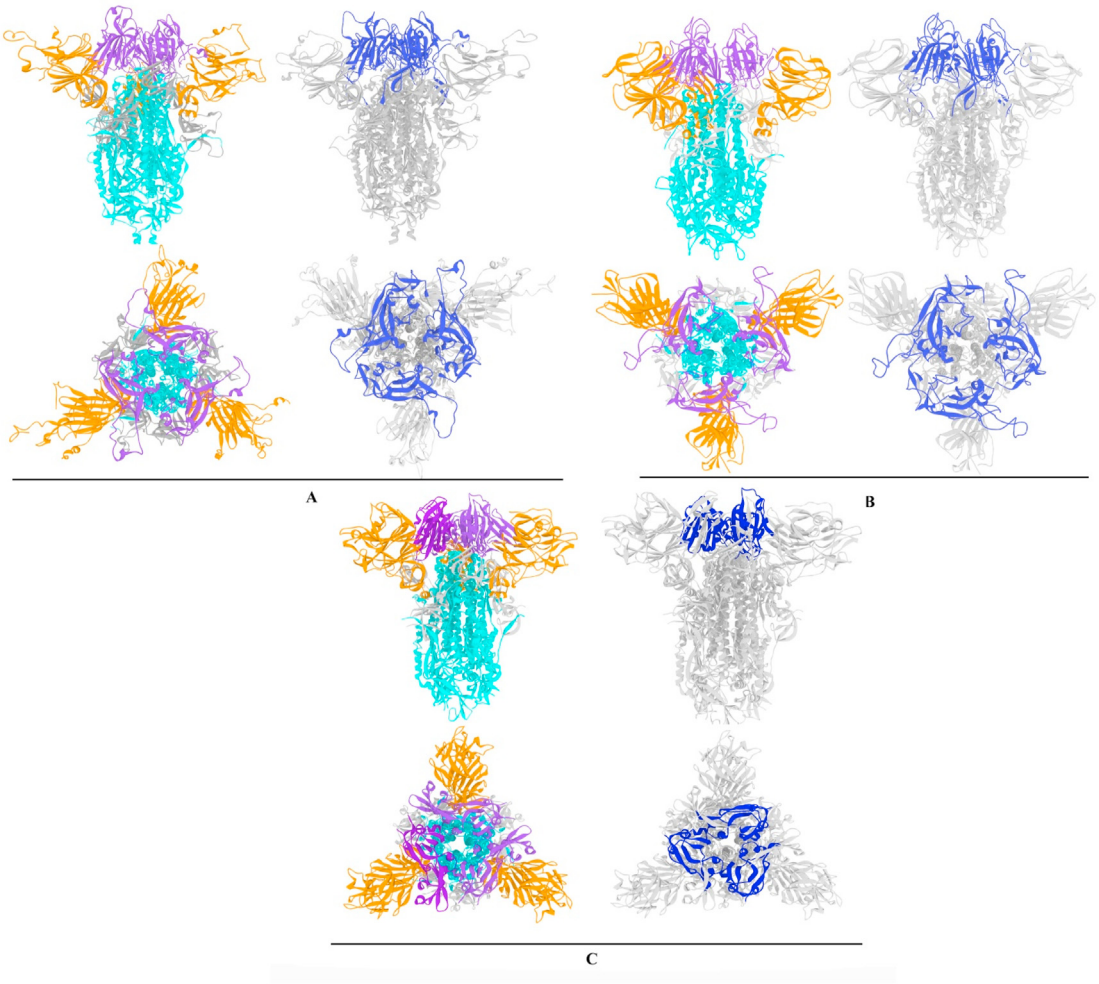

Fig. 2. Important functional domains of Spike glycoprotein of A) SARS-CoV-2, B) SARS-CoV C) MERS-CoV. Upper panel shows the vertical view and the lower panel shows the orthographic top view of the spike. Color coding is as follows: Orange: S1 NTD, Violet: S1 CTD, Cyan: S2 region and Blue: RBD. (For interpretation of the references to color in this figure legend, the reader is referred to the Web version of this article.)

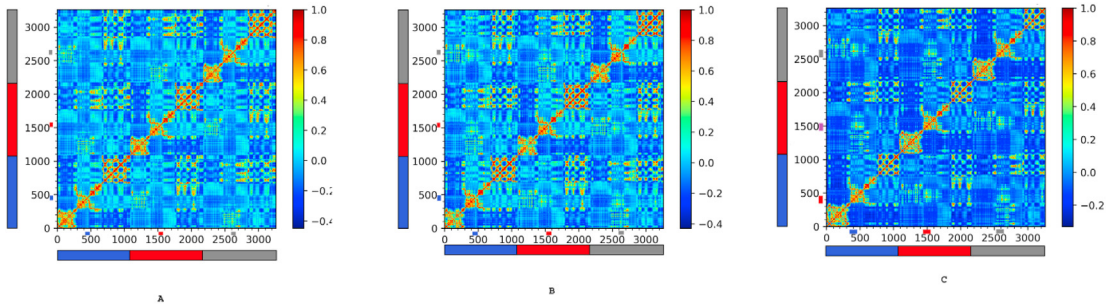

Fig. 3. Cross correlation matrix (CCM) obtained from the first 100 non-zero modes of S protein of (A) SARS-CoV, (B) SARS-CoV-2 and (C) MERS-CoV. Each cell in the matrix depicts the correlation between the motions of two Cα atoms in the protein on a range from −1 (anticorrelated, dark blue) to +1 (correlated, dark red) with 0 conferring no correlation. The horizontal colored bars represent the chain IDs in the trimer as chain A (Blue), chain B(Red), chain C(grey). (For interpretation of the references to color in this figure legend, the reader is referred to the Web version of this article.)

chains which is true for both SARS-CoV and SARS-CoV-2 S protein but variation is seen in the CCM of MERS-CoV S protein (Fig. 3C). S1 NTD of each chain is negatively correlated with NTD of other chains with magnitude range −0.2 to −0.4 but CTD shows weak positive correlation with the CTD of other chains. NTD and CTD belonging to same chain and different chain show similar correlation pattern for SARS-CoV and SARS-CoV-2.

To further stress the nature of correlated dynamics of the RBM (in case of SARS-CoV and SARS-CoV-2) or RBD (in case of MERS-CoV), we have extracted the CCM of the receptor binding region of each S protein model and plotted as heat map (Fig. 4). A common fact is that RBM or RBD of different chains show indistinguishable concerted movements for a particular S protein. In case of SARS-CoV-2 S, two ranges of correlations are seen in the CCM: weak

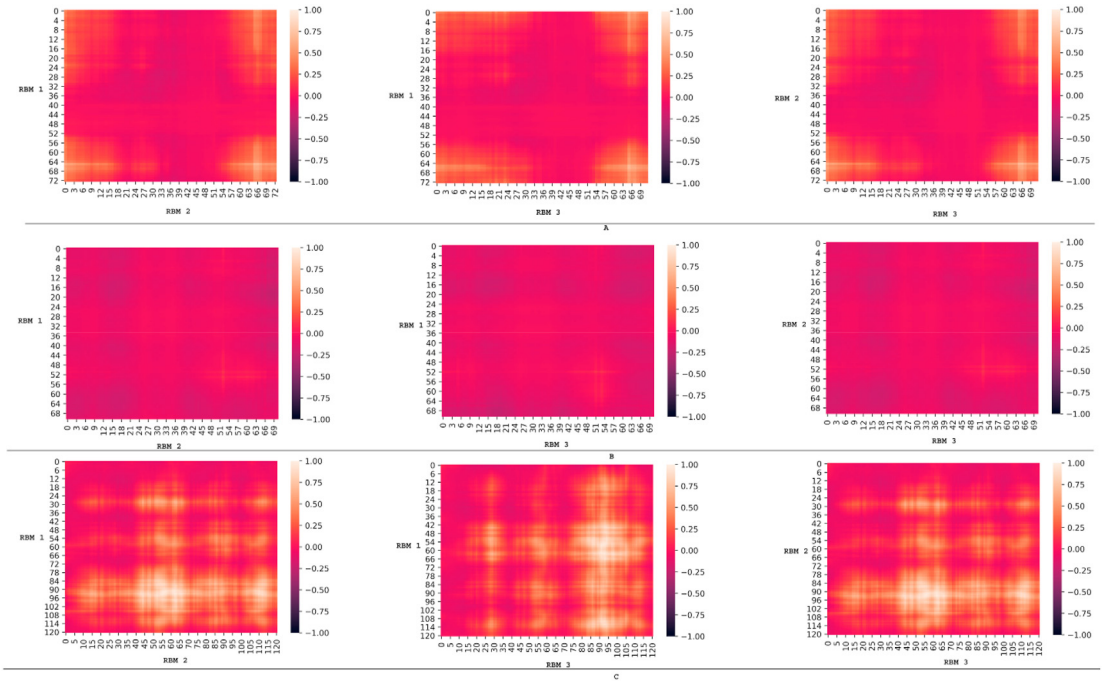

Fig. 4. CCM of the RBM (for SARS-CoV, SARS-CoV-2) and RBD (MERS-CoV) extracted from Fig. 2. The CCM is plotted using Seaborn python module and the color intensity values corresponds to Fig. 2. A) CCM of SARS-CoV-2, B) CCM of SARS-CoV and C) CCM of MERS-CoV S protein. RBM 1, 2, 3 or RBD 1, 2, 3 corresponds to the domains of chain A, B, C respectively. (For interpretation of the references to color in this figure legend, the reader is referred to the Web version of this article.)

positive (0–0.25) and strong positive (0.5–1) (Fig. 4A). Overall weak negative correlation (−0.1 to −0.5) is noticed between the RBMs of SARS-CoV S (Fig. 4B) and dominance of very strong correlation is observed among the RBDs of MERS-CoV S protein (Fig. 4C).

Displacement vectors of atoms for individual normal modes provide significant information about the protein dynamics and these vectors are unique to a particular normal mode. The low frequency normal modes show collective motions of the amino acids which are related to the functional movements of proteins such as opening and closing motions and sliding motions around the interfaces of domains [32]. In order to comprehensibly describe the motion of the trimer chains of the first four low frequency (low eigenvalue) modes (λ_7, λ_8, λ_9, λ_{10}), first we have computed three unique symmetry axis of the spike trimer using VMD Symmetry Tool. Among the three symmetry axis, one pointed outward through the trimer core, which we have named the Z axis (default 2 in VMD nomenclature) and the other two axis were named as X and Y axis (default VMD nomenclature 1 and 0 respectively). We have used default PDB chain ids of the three spike protein structures to address the chain and trimer motion individually. As previously described we will confined ourselves to discuss the motion of S1 domain of the three chains as it harbors the functional receptor binding domain. In all the structures, the β-strand region (BSR) of S1 dominates overall motions of the trimer in first four low frequency non-zero modes (**supplementary 4, 5 and 6**). We did not notice any concerted motion of the three chains (i.e. move in a same direction) in the mentioned modes of all the three structures. In SARS-CoV-2 spike mode 1 (λ_7), chain A, B and C shows rotational motion around the Z symmetry axis but direction is not coherent. In order to quantitatively characterize the mutual directionality of the domains of each chain, we have computed the cosine similarity (CS) which will give an intuition about the similarity measure between the displacement vectors and positive/negative sign will highlight the direction of the Cα atom motion. BSR of chain A and B move in parallel with the XY plane merely in the same direction (CS value of 0.26) whereas BSR of chain C shows an upward translational motion from XY plane (at an angle of 35˚-45˚) and in opposite direction of chain B BSR (CS value of −0.8). RBM of chain A, B and C shows somewhat unidirectional translational motion along negative Y direction (CS value of 0.48 between A and B, 0.40 between A and C and 0.61 between B and C) but a bending motion is seen in RBM of chain B and C. In chain C RBM, segment Ser469 to Gly482 has opposite directional movement than rest of the RBM. Mode 2 (λ_8) has exact similar kind of dynamics as mode 1 except chain B and chain C BSR move in same direction in parallel with XY plane (CS value of 0.35) and chain A BSR shows upward translational motion from XY plane. All three RBM shows unidirectional translational motion along XY plane. RBM of chain A and chain C move in mere exact same direction with CS value of 0.72. No bending motion is seen the RBM of all the chains. In mode 3 (λ_9), predominant translational motion is seen in chain C RBM along Z axis. In mode 4 (λ_{10}), a complete rotational motion of the BSRs around Z axis in the clockwise fashion is seen. RBM of all the chains show discontinuous motion with very low magnitude (supplementary 5). In mode 1 of SARS-CoV spike, we found a very strong colliding motion of chain B and C BSR (CS value of −0.76) and chain A BSR produces somewhat translational motion along the negative Z axis through XY plane which is unique than SARS-CoV-2 spike mode 1. Another striking difference comes from the motion of the RBM. Chain A and chain B RBM shows collision type motion with one another (CS value −0.31) which is absent in SARS-CoV-2 spike. Chain A RBM does not show unidirectional motion as the other two chains do. Pro446-Trp463, Tyr481-Pro494 and Gly469-Tyr481 produce varying vector directionality. In mode 2, there occurs some similarity with SARS-CoV-2 spike BSR motion in mode 1: chain A and C BSR shows unidirectional motion parallel to XY plane (CS value of 0.26) and chain B BSR is pushed towards the trimer core. BSRs of all the chain shows anticlockwise rotational motion in mode 3 and the RBMs tend to coalesce into trimer core which could be regarded as

closing motion. In mode 4 chain B and C BSR move in a same direction (negative XY plane) (CS value of 0.65) and takes the RBMs in the same direction as a result these two chain tends to open the trimer core. On the other hand, chain A RBM is pushed towards the core to fill the void produced by other two chains. In all the four described modes, RBM does not show any kind of translational motion along the positive Z axis (supplementary 4). Overall spike motion of MERS-CoV spike in all the four modes seems to be mere similar with SARS-CoV and SARS-CoV-2 but some differences persist. In mode 1 chain B and C BSR shows translational motion along parallel to XY plane in the same direction (CS value of 0.39) whereas chain A BSR moves towards the negative Z axis. RBDs of all the chains move along in the same direction (parallel to 4th quadrant of XY plane). Mode 2 shows high degree of similarity with mode 1. This time chain A and B BSR move unidirectional (CS value of 0.22) parallel to XY plane and chain C BSR shows upward translational motion along positive Z axis (approximate 90° from XY plane). All the RBD shows strong unidirectional motion along third quadrant of XY plane. In mode 3, some sort of unclear clockwise rotational motion around Z axis is seen in all the chains but the RBD seems to stationary. During the rotation, single chains show bending motion. Mode 4 motion is somewhat rearrangement of mode 1 and the RBDs move in the same direction (along the first quadrant of XY plane) with similar CS value (0.64 ± 0.05) (supplementary 6). In Fig. 5 we have projected the eigenvectors of the first four non-zero low frequency normal modes (λ_7, λ_8, λ_9, λ_{10}) on to the Cα backbone atom.

3.3. Atomic fluctuations of the trimeric S protein of SARS-CoV-2, SARS-CoV and MERS-CoV

We have computed the squared atomic fluctuations of the S protein models using first 10 non-zero normal modes (Fig. 6). The amplitude of the fluctuations shows variation within the models. In SARS-CoV S, the three chains have exact similar fluctuation pattern as if they are mirror image to each other. Region 404–504 which include the RBM, has much lower mean atomic displacement (although residues 441–450 of all the three chains show high fluctuation) than the β-strand region (14–290) which is also evident from the vector representation (Fig. 5A). Mean atomic fluctuation of the NTD β-strand region (18–267) and RBM (437–508) of SARS-CoV-2 S is much higher compared to the SARS-CoV and MERS-CoV S. There are some localized differences which are worth discussing. Highest fluctuation in SARS-CoV S comes from residue Leu486 (0.32) in all the chains. In SARS-CoV-2 S high mobility comes from following residues: Glu156 (2.76) of chain A, Met153 (2.34) and Cys480 (3.25) of chain B, Arg158 (2.58) and Gly485 (2.28) of chain C. In MERS-CoV S highest fluctuation comes from a single residue of two different chains: Pro761 in chain A and C which is obviously part of S2 region. When the fluctuation of the RBM of SARS-CoV S and SARS-CoV-2 S and RBD of MERS-CoV were magnified for deeper analysis, a noticeable scenario appears. In SARS-CoV and MERS-CoV S the RBM and RBD respectively of all the chains have perfectly overlapped atomic fluctuation but wide variation is spotted in SARS-CoV-2 S where RBM of all the chains do not fluctuates in a synchronized fashion (Fig. 7). When atomic fluctuation of the standing state spike of SARS-CoV and SARS-CoV-2 was computed, it was found that the RBM of later has higher mean atomic fluctuation than the former (Supplementary).

3.4. Comparative analysis on the normal modes of the trimeric S protein of SARS-CoV-2, SARS-CoV and MERS-CoV

In order to compare the normal modes between the structures, we have calculated the RMSIP, spectral overlap using the first 100 non-zero normal modes and plotted the cosine correlation between the modes of the structures. As chain A, B and C of one spike protein does not correspond to the same in other spike, we have computed all possible combination. Chain A, B and C have six possible combinations (ACB, BAC, BCA, CAB, CBA, ABC and the naming are 1,2,3,4,5,6 respectively) and during quantitative comparison between two structures, all the mentioned combinations has been taken account and average value was computed. As RMSIP and spectral overlap do not consider vector dimensionality, single combination computation is sufficient to draw conclusion. From Table 1 it is evident that there is very little similarity present in terms of the normal modes between the S proteins of the mentioned viruses due to very low RMSIP and spectral overlap values. The values do not deviate much from the default chain id values. We also noticed a negative correlation between RMSD and the computed RMSIP, spectral overlap values. In spite of having structural differences we have explored for any modes which are similar between the S protein models. Overlap plots were also calculated for every chain combination (supplementary). Very low overlap values between the modes of SARS-CoV and MERS-CoV spike and SARS-CoV-2 and MERS-CoV spike indicates very low similarities in the motions of the spike in all chain combinations. In case of SARS-CoV and SARS-CoV-2, overlap values greater than 0.6 is found in first two non-zero normal modes in one of the combinations (Supplementary) indicating mere identical global motions. In Fig. 9 we have plotted the overlap values of the mentioned spike proteins for pictorial overview where the default PDB chain ids were used. For example, a very low overlap value of 0.36 between λ_{16} of MERS-CoV and λ_{37} of SARS-CoV spike is noticed (Supplementary animation 1,2,3,4) indicating they have no common global collective motions. So, overlap values can reveal detailed similarities or dissimilarities between the modes of two comparing protein structures. Overlap plots of the other combinations We also compared the normal modes of lying and standing states of SARS-CoV and SARS-CoV-2 (Fig. 8) spike and previously explained chain id combinations was also used to compute RMSIP, spectral overlap and cosine correlation. We found that default PDB chains id of this two conformations of spike has highest RMSIP and spectral overlap values indicating high level of similarity between the modes. Overlap matrix also confirms this fact (Supplementary).

Supplementary video related to this article can be found at https://doi.org/10.1016/j.jmgm.2020.107778

4. Discussion

Normal mode analysis of equilibrium structures falls in the category of principal component analysis-based methods like singular value decomposition of molecular dynamics or Monte Carlo trajectories or essential dynamics analysis of the covariance matrices retrieved from MD runs [20]. These studies have proven to be useful in studying the equilibrium dynamics of proteins which are spanned by low frequency end of the mode spectrum [33]. Anisotropic network model (ANM), a category of elastic network model (ENM), has been previously evaluated on a large set of proteins to obtain optimal model parameters to achieve best correlation with experimental datasets and it is shown that protein residue fluctuations can be accurately predicted by this model which is in well agreement with the experiments [34]. Spike glycoprotein or S protein of MERS-CoV, SARS-CoV and SARS-CoV-2 is the major determinant of viral tropism and is responsible for receptor binding and membrane fusion to cause severe pulmonary diseases which often leads to fatality. Detailed studies on the atomic motions of the S protein will enable us to gain information about different conformations of this protein which will ultimately lead to the identification of possible inhibitor binding sites and

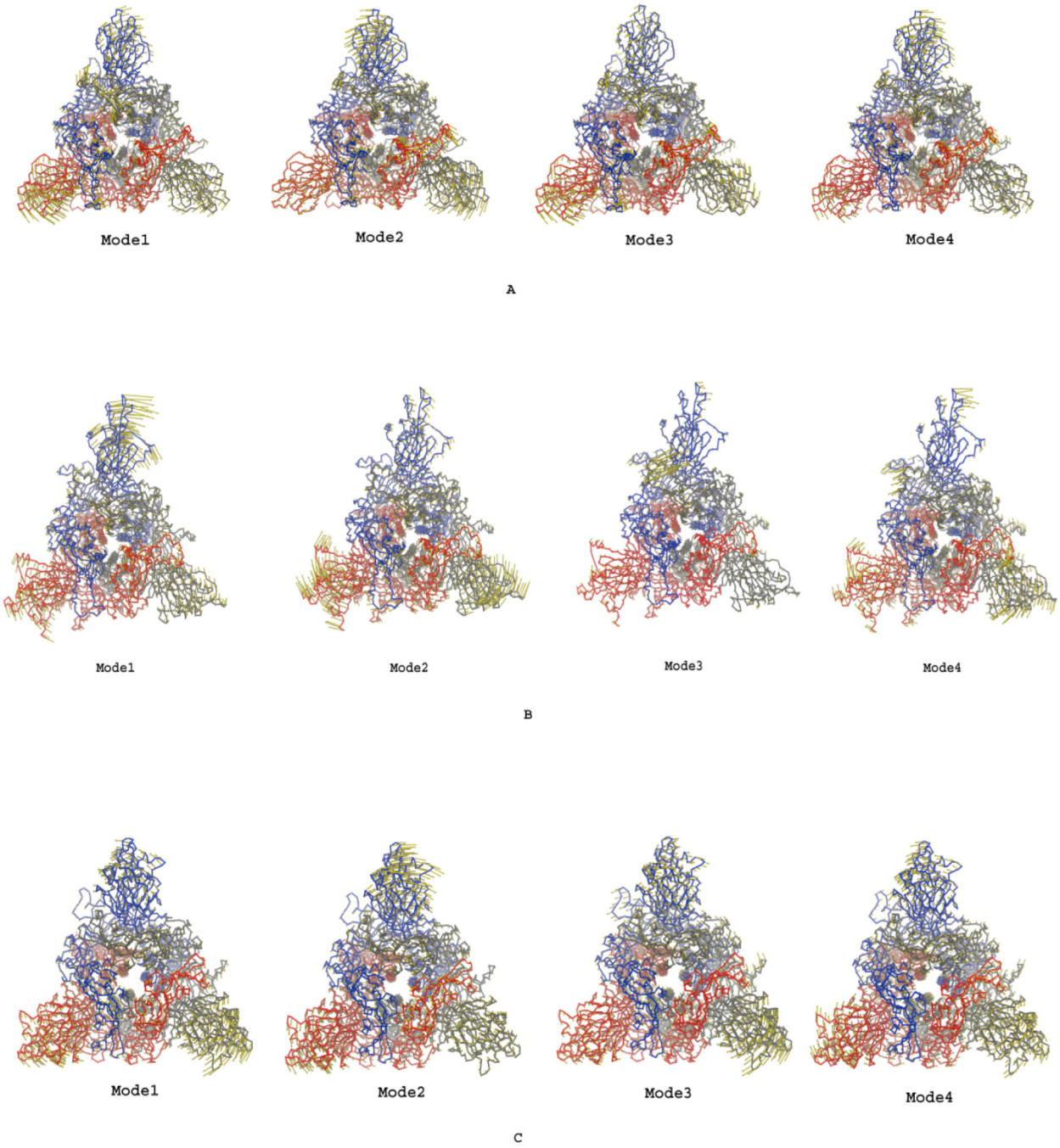

Fig. 5. Orthographic top view of the S protein of (A) SARS-CoV, (B) SARS-CoV-2, (C) MERS-CoV. Eigenvectors of first four non-zero normal modes are projected on Cα backbone atom. Yellow arrows indicate the direction of the vectors and length indicates the magnitude of displacement of the respective normal mode (vector values corresponds to particular mode and the scale is not same). (For interpretation of the references to color in this figure legend, the reader is referred to the Web version of this article.)

designing of proper inhibitors. In this study we have used NMA study to characterize the motions and correlated dynamics within the S protein structure of MERS-CoV, SARS-CoV and SARS-CoV-2. We compared the motions of the three proteins with each other to better understand their dynamics. Previously ANM was used to characterize global mode shape of Gramicidin A, a membrane protein, and it was found that the model obtained from the calculation was as accurate as that obtained from CHARM22 force field [35]. We have taken the prefusion, lying state conformations of the S proteins of MERS-CoV, SARS-CoV and SARS-CoV-2 for the NMA study. From the frequency data of the normal modes we can get our first intuition about the variation in the global as well as small localized movements of the Cα backbone atoms of S protein models. The low frequency modes are of great interest to determine most probable global fluctuations of protein molecule as large eigenvalues (high frequency modes), which is proportional to energy, will lead to energetically unfavorable motions [20]. Spectra of eigenvalues shows that SARS-CoV-2 S has more collective motion than other two S protein implying SARS-CoV-2 S protein has higher stability [32] and has lower energetically expensive motion than the latter. This stability of the S trimer of SARS-CoV-2 in terms of eigenvalue frequency may give a part of the explanation about why

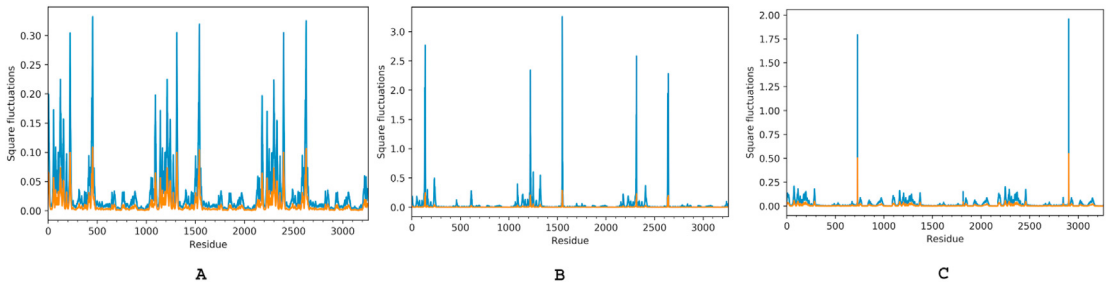

Fig. 6. Atomic fluctuations of the S protein for A) SARS-CoV, B) SARS-CoV-2 C) MERS-CoV. Residue index (X co-ordinate) is different for each model as the excluded portions are different but all have same numbers of C_α atoms (3261). The X coordinates in the plots are continuous but are divided in three chains consecutively by 1087 C_α atoms. Index 0 in SARS-CoV is equal to 5 and 1087 is equal to 1091; Index 0 in SARS-CoV-2 is equal to 18 and 1087 is equal to 1104; Index 0 in MERS-CoV is equal to 33 and 1087 is equal to 1119. Y axis represents the squared atomic fluctuation (Blue) and Normalised atomic fluctuation (Orange). (For interpretation of the references to color in this figure legend, the reader is referred to the Web version of this article.)

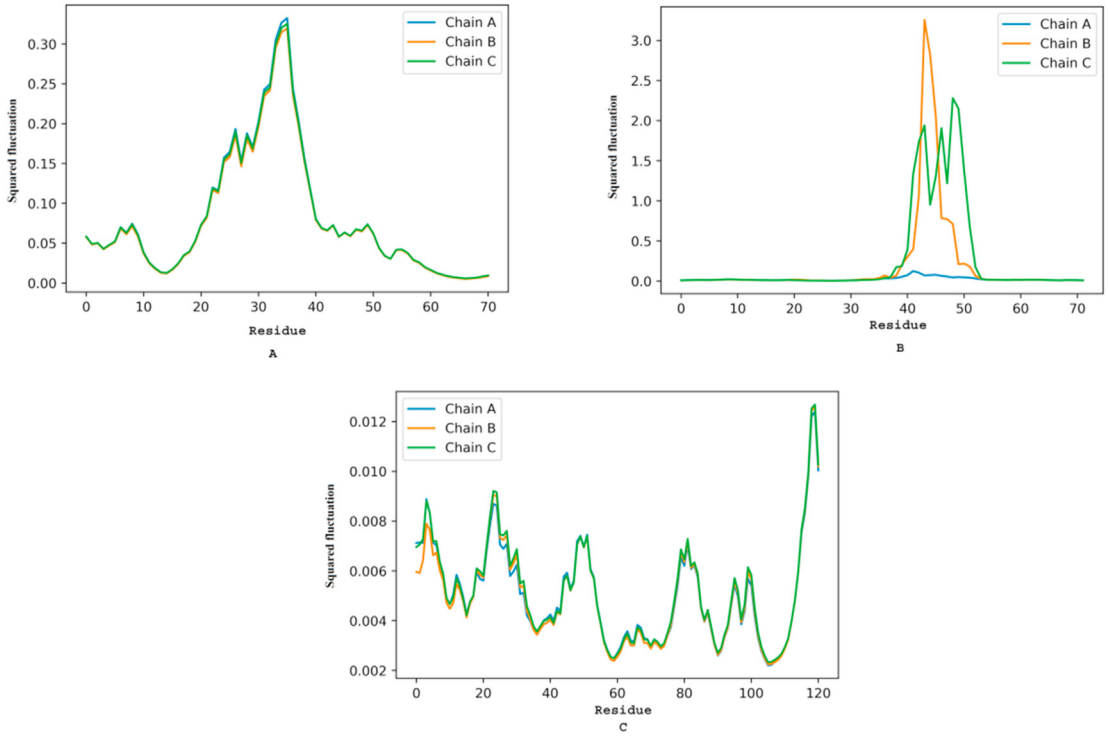

Fig. 7. Squared fluctuations of the RBM of (A) SARS-CoV, (B) SARS-CoV-2 and RBD of (C) MERS-CoV. Y axis is the squared fluctuation and X axis is the residue index for all the plots.

Table 1
Comparison of normal modes of different S protein models.

Compared Models (S protein)	RMSIP	Spectral Overlap	RMSD between the models (Å)	Sequence Identity (%)
SARS-CoV and MERS-CoV	0.33 ± 0.004	0.07 ± 0.008	5.377	30.67
SARS-CoV and SARS-CoV-2	0.39 ± 0.02	0.11 ± 0.02	1.840	73.98
MERS-CoV and SARS-CoV-2	0.31 ± 0.005	0.06 ± 0.004	3.951	35.54

SARS-CoV-2 is more infective than other two but do not provide detailed description. It is shown that in SARS-CoV S, which is the lying state, the RBD is buried in the S protein trimer therefore interaction with ACE receptor is hindered. In order to bind with receptor, S protein must switch to standing state where RBD of any one of the chains is exposed and binds with receptor [8] (Fig. 8). From the homogenous CCM plot of whole trimer (Fig. 2), we hypothesize that the molecular mechanism of this conformational switching at atomic scale may be similar in nature in the three viruses but the variation seen in the CCM of RBM and RBD are responsible for the difference in infectivity. It can be said from the CCM that RBD of all three chains have equal probability to be switched into standing state. From the first four low frequency non-zero modes (λ_7, λ_8, λ_9, λ_{10}) localized variation in the direction of C_α atom motion in the models are worth noticeable (Fig. 5). We have also described the motions of the C_α respect to the symmetry axis of the trimer (supplementary 4,5,6). The β-sandwitch region in all the three S protein models shows various translational motions respects to the XY plane or clockwise and anticlockwise rotational motion around the Z axis which serves the basis of overall intrinsic

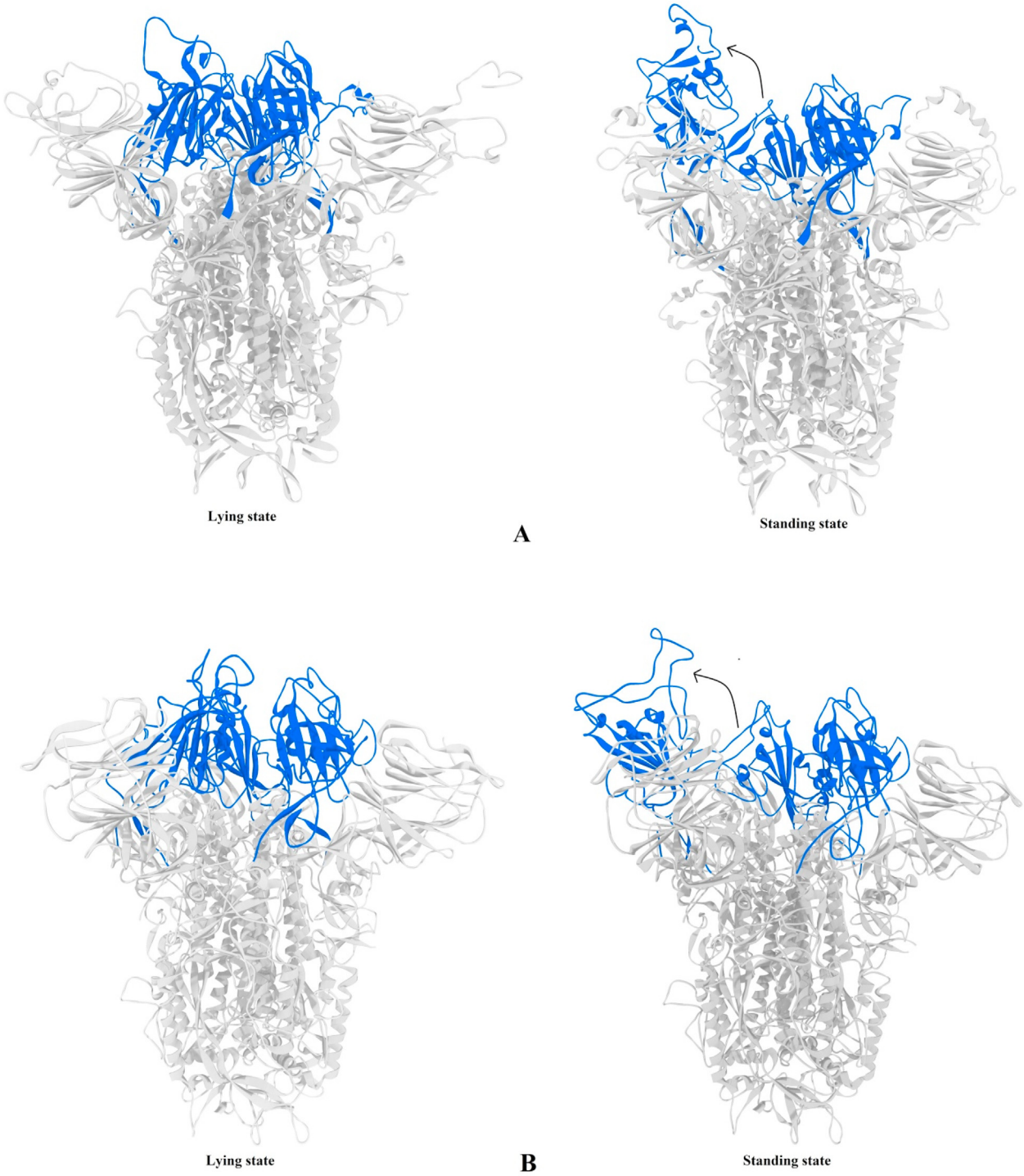

Fig. 8. Closed or lying state and open or standing state of spike protein of A) SARS-CoV-2 and B) SARS-CoV. In both cases one of the three RBDs is switched into open state and all three RBDs have equal probability to be switched into this conformation.

dynamics and constitutes the variability in motions in the S protein models. Complete rotational motion (clockwise or anticlockwise) of the chains around Z axis is scarce in all the S protein structures. The RBD or RBM also shows variation in C_α vector directionality in said spike proteins which also serves the basis of marked dynamic variation. In mode 3 (λ_9) of SARS-CoV-2 S protein, dominant motion comes from the RBM motif of chain A, especially Phe486. A recent MD simulation study shows that CR1 loop of RBD of SARS-CoV S protein is more rigid than that of SARS-CoV-2 and this high flexibility of CR1 in SARS-CoV-2 S protein anchors Phe486 deep into the hydrophobic pocket of ACE2 receptor. This leads to more tight binding of SARS-CoV-2 S protein RBD to the receptor than SARS-CoV and it explains partially, why SARS-CoV-2 is 10–15 times more infective than SARS-CoV [31]. Cryo-EM studies have shown that, in SARS-CoV spike, the RBD is mostly in the standing state [8,11] however, in SARS-CoV-2 spike, the RBD is mostly in the lying

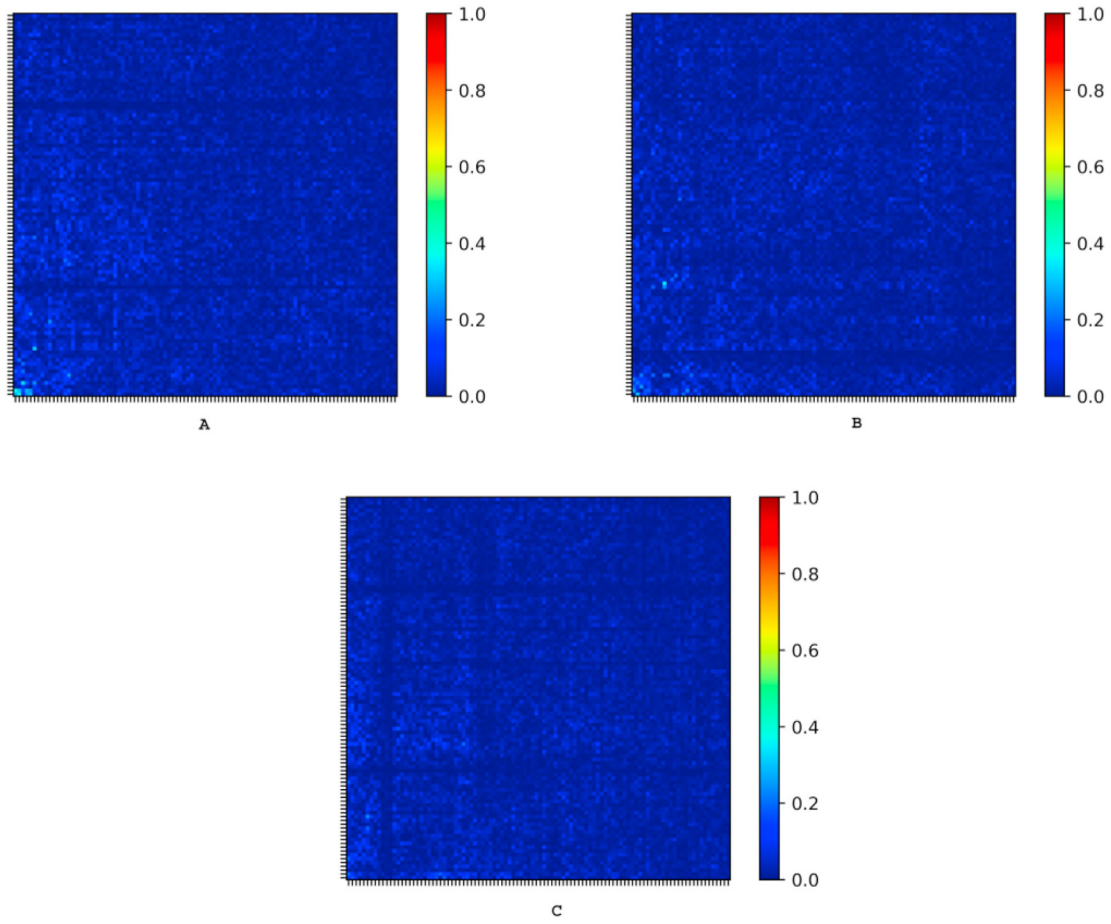

Fig. 9. Cosine correlation or Overlap between the modes of different S protein models with default PDB chain ids. X and Y axis represents the normal mode indices of the respective models and each cell in the matrix shows the overlap or Cosine correlation value on a range from 0 (no overlap) to 1 (fully overlapped). Each plot shows the heatmap of overlap matrix between S protein of **(A)** SARS-CoV and SARS-CoV-2, **(B)** SARS-CoV and MERS-CoV, **(C)** SARS-CoV-2 and MERS-CoV.

state [36] thus the probability of infection should be more for SARS-CoV than SARS-CoV-2. But from this study it can be said that the intrinsic nature of the high flexibility of the RBD (especially the RBM) of one of the chains increases the probability of the spike to bind with the ACE2 receptor through multiple hydrophobic bonds before switching to standing state. In standing state, the RBD of SARS-CoV and SARS-CoV-2 spike protein shows higher atomic fluctuation in order to be accessible to the ACE2 receptor which supports the MD simulation data. The variation in the β-sandwich region of MERS-CoV S due to grafting of distinct variable loops, results in the variation in dynamics of the first four non-zero normal modes as well as in the magnitude of atomic fluctuations. In order to find any type of similarity in the dynamics of different modes we have computed overlap matrix using the first 100 non zero modes of the models. During the comparison of modes between the oligomer structures, issue of chain identifiers must be addressed. In other words, when the two modes are compared, chains A, B, and C in one protein (or mode) are not necessary to correspond to chains A, B, and C in another protein (or mode).So, all possible chain combinations of the spike are used during comparison between two S proteins. For example, when modes of SARS-CoV and MERS-CoV spike are compared, we produced six possible chain combinations of MERS-CoV S: ABC(default PDB id), $AC_{(B)}B_{(C)}$, $B_{(A)}A_{(B)}C$, $B_{(A)}C_{(B)}A$, $C_{(A)}A_{(B)}B_{(C)}$, $C_{(A)}B_{(B)}A_{(C)}$ where ABC is the default PDB chain ID. $B_{(A)}A_{(B)}C$ means in this new chain ID chain B in default id is now given as chain A identifier, chain A in default id is now given as chain B identifier and chain C is not changed. Average value was calculated for RMSIP and spectral overlap using the six chain combinations in each comparison. Overlap plot was also created for all combinations (supplementary 7,8,9). Overlap plot of SARS-CoV-2 and SARS-CoV spike combination $B_{(A)}C_{(B)}A$ shows high overlap value (>0.5) in first five non-zero normal mode indicating similar trend in global C_α atom motion. Very low overlap values between SARS-CoV and MERS-CoV, SARS-CoV-2 and MERS-CoV spike in all chain combinations indicates absence of similarity in C_α atom motion both in low as well as higher normal mode index. Similar chain combinations was also used in comparison of lying and standing state of SARS-CoV and SARS-CoV-2 spike. High RMSIP and spectral overlap value was found in default PDB chain id and rest of the values are far from this value in both structures. In SARS-CoV spike lying and standing state, computed RMSIP and spectral overlap value is 0.75 and 0.36 and in SARS-CoV-2 spike lying and standing state, computed RMSIP and spectral overlap value is 0.88 and 0.48 respectively. High overlap values along the diagonal of the matrix suggests that in lying and standing state of SARS-CoV and SARS-CoV-2 spike, overall intrinsic dynamics remains similar supporting our finding that even in lying state there is a chance of binding with the receptors due to high flexibility of the RBM. Very low RMSIP and spectral overlap values involving MERS-CoV S protein indicates very different kinds of atomic displacement than the other models. These characteristics of MERS-CoV S protein dynamics is obvious because of the distal placement of MERS-CoV S

protein in phylogenetic tree from SARS-CoV and SARS-CoV-2 S protein [35]. This study unravels the intrinsic difference between the S proteins of three viruses which is manifested in the form of varying degrees of infectivity.

5. Conclusions

The present comprehensive study demonstrated the intrinsic dynamics of the S proteins from SARS-CoV-2, SARS-CoV and MERS-CoV and their inter-relationship through normal mode analysis using ANM. High fluctuation of the RBM of SARS-CoV-2 spike indicates its propensity to bind with ACE2 even in the lying state inferring its higher infectivity than SARS-CoV and MERS-CoV. The distant relationship of MERS-CoV with the SARS-CoV and SARS-CoV-2 in phylogenetic tree at sequence level resembles that at the dynamics level due to its unique dynamical motion. Sites of very low atomic fluctuation at the S1 site which harbours the RBD could serve as the potential drug binding site. Our study could serve as the basis for designing common potential drugs against the spike of the three mentioned viruses which may inhibit the conformational changes from lying to standing state.

Author contributions

Protocol designed, conceptualized and analyzed by S.M., manuscript preparation done by D.C. and J.D. Project was done under the supervision of K.G. The manuscript was reviewed and approved by all authors.

Declaration of competing interest

The authors declare that they have no known competing financial interests or personal relationships that could have appeared to influence the work reported in this paper.

Acknowledgment

This study was supported by FRPDF grant of Presidency University.

Appendix A. Supplementary data

Supplementary data to this article can be found online at https://doi.org/10.1016/j.jmgm.2020.107778.

References

[1] M.A. Shereen, S. Khan, A. Kazmi, N. Bashir, R. Siddique, COVID-19 infection: origin, transmission, and characteristics of human coronaviruses, J. Adv. Res. 24 (2020) 91–98, https://doi.org/10.1016/j.jare.2020.03.005.
[2] V.D. Menachery, R.L. Graham, R.S. Baric, Jumping species—a mechanism for coronavirus persistence and survival, Curr. Opin. Virol. 23 (2017) 1–7, https://doi.org/10.1016/j.coviro.2017.01.002.
[3] WHO, Summary of Probable SARS Cases with Onset of Illness from 1 November 2002 to 31 July 2003, WHO, 2015.
[4] Middle East respiratory syndrome coronavirus (MERS-CoV) (n.d.), https://www.who.int/news-room/fact-sheets/detail/middle-east-respiratory-syndrome-coronavirus-(mers-cov (accessed June 4, 2020).
[5] T.R.F. Smith, A. Patel, S. Ramos, D. Elwood, X. Zhu, J. Yan, E.N. Gary, S.N. Walker, K. Schultheis, M. Purwar, Z. Xu, J. Walters, P. Bhojnagarwala, M. Yang, N. Chokkalingam, P. Pezzoli, E. Parzych, E.L. Reuschel, A. Doan, N. Tursi, M. Vasquez, J. Choi, E. Tello-Ruiz, I. Maricic, M.A. Bah, Y. Wu, D. Amante, D.H. Park, Y. Dia, A.R. Ali, F.I. Zaidi, A. Generotti, K.Y. Kim, T.A. Herring, S. Reeder, V.M. Andrade, K. Buttigieg, G. Zhao, J.-M. Wu, D. Li, L. Bao, J. Liu, W. Deng, C. Qin, A.S. Brown, M. Khoshnejad, N. Wang, J. Chu, D. Wrapp, J.S. McLellan, K. Muthumani, B. Wang, M.W. Carroll, J.J. Kim, J. Boyer, D.W. Kulp, L.M.P.F. Humeau, D.B. Weiner, K.E. Broderick, Immunogenicity of a DNA vaccine candidate for COVID-19, Nat. Commun. 11 (2020) 2601, https://doi.org/10.1038/s41467-020-16505-0.
[6] M.A. Tortorici, D. Veesler, Structural insights into coronavirus entry, in: Adv. Virus Res., Academic Press Inc., 2019, pp. 93–116, https://doi.org/10.1016/bs.aivir.2019.08.002.
[7] R.N. Kirchdoerfer, C.A. Cottrell, N. Wang, J. Pallesen, H.M. Yassine, H.L. Turner, K.S. Corbett, B.S. Graham, J.S. McLellan, A.B. Ward, Pre-fusion structure of a human coronavirus spike protein, Nature 531 (2016) 118–121, https://doi.org/10.1038/nature17200.
[8] M. Gui, W. Song, H. Zhou, J. Xu, S. Chen, Y. Xiang, X. Wang, Cryo-electron microscopy structures of the SARS-CoV spike glycoprotein reveal a prerequisite conformational state for receptor binding, Cell Res. 27 (2017) 119–129, https://doi.org/10.1038/cr.2016.152.
[9] X.Y. Ge, J.L. Li, X. Lou Yang, A.A. Chmura, G. Zhu, J.H. Epstein, J.K. Mazet, B. Hu, W. Zhang, C. Peng, Y.J. Zhang, C.M. Luo, B. Tan, N. Wang, Y. Zhu, G. Crameri, S.Y. Zhang, L.F. Wang, P. Daszak, Z.L. Shi, Isolation and characterization of a bat SARS-like coronavirus that uses the ACE2 receptor, Nature 503 (2013) 535–538, https://doi.org/10.1038/nature12711.
[10] R.N. Kirchdoerfer, N. Wang, J. Pallesen, D. Wrapp, H.L. Turner, C.A. Cottrell, K.S. Corbett, B.S. Graham, J.S. McLellan, A.B. Ward, Stabilized coronavirus spikes are resistant to conformational changes induced by receptor recognition or proteolysis, Sci. Rep. 8 (2018), https://doi.org/10.1038/s41598-018-34171-7.
[11] Y. Yuan, D. Cao, Y. Zhang, J. Ma, J. Qi, Q. Wang, G. Lu, Y. Wu, J. Yan, Y. Shi, X. Zhang, G.F. Gao, Cryo-EM structures of MERS-CoV and SARS-CoV spike glycoproteins reveal the dynamic receptor binding domains, Nat. Commun. 8 (2017) 1–9, https://doi.org/10.1038/ncomms15092.
[12] H. K, T. A, F. Mj, Analysis of domain motions in large proteins, Proteins 34 (1999) 369–382, https://doi.org/10.1002/(SICI)1097-0134(19990215)34:3<369::AID-PROT9>3.0.CO;2-F.
[13] K. Hinsen, Analysis of domain motions by approximate normal mode calculations, Proteins Struct. Funct. Bioinforma. 33 (1998) 417–429, https://doi.org/10.1002/(SICI)1097-0134(19981115)33:3<417::AID-PROT10>3.0.CO;2-8.
[14] I. Bahar, T.R. Lezon, L.-W. Yang, E. Eyal, Global dynamics of proteins: bridging between structure and function, Annu. Rev. Biophys. 39 (2010) 23–42, https://doi.org/10.1146/annurev.biophys.093008.131258.
[15] A.M. Strom, S.C. Fehling, S. Bhattacharyya, S. Hati, Probing the global and local dynamics of aminoacyl-tRNA synthetases using all-atom and coarse-grained simulations, J. Mol. Model. 20 (2014) 1–11, https://doi.org/10.1007/s00894-014-2245-1.
[16] L.W. Yang, E. Eyal, C. Chennubhotla, J.G. Jee, A.M. Gronenborn, I. Bahar, Insights into equilibrium dynamics of proteins from comparison of NMR and X-ray data with computational predictions, Structure 15 (2007) 741–749, https://doi.org/10.1016/j.str.2007.04.014.
[17] I. Bahar, A.J. Rader, Coarse-grained normal mode analysis in structural biology, Curr. Opin. Struct. Biol. 15 (2005) 586–592, https://doi.org/10.1016/j.sbi.2005.08.007.
[18] Normal mode analysis: theory and applications to biological and chemic, n.d. https://www.routledge.com/Normal-Mode-Analysis-Theory-and-Applications-to-Biological-and-Chemical/Cui-Bahar-Gross-Lenhart-Maini-Etheridge-Voit-Ranganathan-Safer-Bowman-Brooks-Hinsen-Jernigan-Keyes-Kitao-Leitner-Liu-Ma-Nilges-Olson-Perahia-Phillips-Jr-Sanejouand-Straub-van-Vlijmen-Tama-Rader-Chennubhotla-Yang-Yu-Matsumoto-Li/p/book/9781584884729 (accessed July 9, 2020)
[19] E. Eyal, L.-W. Yang, I. Bahar, Anisotropic Network Model: Systematic Evaluation and a New Web Interface, vol. 22, 2006, pp. 2619–2627, https://doi.org/10.1093/bioinformatics/btl448.
[20] I. Bahar, T.R. Lezon, A. Bakan, I.H. Shrivastava, Normal mode analysis of biomolecular structures: functional mechanisms of membrane proteins, Chem. Rev. 110 (2010) 1463–1497, https://doi.org/10.1021/cr900095e.
[21] Protein Data Bank | Nucleic Acids Research, Oxford Academic, (n.d.), https://academic.oup.com/nar/article/28/1/235/2384399. accessed July 8, 2020.
[22] Y.-J. Park, A.C. Walls, Z. Wang, M.M. Sauer, W. Li, M.A. Tortorici, B.-J. Bosch, F. DiMaio, D. Veesler, Structures of MERS-CoV spike glycoprotein in complex with sialoside attachment receptors, Nat. Struct. Mol. Biol. 26 (2019) 1151–1157, https://doi.org/10.1038/s41594-019-0334-7.
[23] A.C. Walls, Y.J. Park, M.A. Tortorici, A. Wall, A.T. McGuire, D. Veesler, Structure, function, and antigenicity of the SARS-CoV-2 spike glycoprotein, Cell 181 (2020) 281–292, https://doi.org/10.1016/j.cell.2020.02.058, e6.
[24] S. Jo, T. Kim, V.G. Iyer, W. Im, CHARMM-GUI: a web-based graphical user interface for CHARMM, J. Comput. Chem. 29 (2008) 1859–1865, https://doi.org/10.1002/jcc.20945.
[25] H. Wako, S. Endo, Normal mode analysis as a method to derive protein dynamics information from the Protein Data Bank, Biophys. Rev. 9 (2017) 877–893, https://doi.org/10.1007/s12551-017-0330-2.
[26] E. Fuglebakk, S.P. Tiwari, N. Reuter, Comparing the intrinsic dynamics of multiple protein structures using elastic network models, Biochim. Biophys. Acta Gen. Subj. 1850 (2015) 911–922, https://doi.org/10.1016/j.bbagen.2014.09.021.
[27] M.E. Dorner, R.D. McMunn, T.G. Bartholow, B.E. Calhoon, M.R. Conlon, J.M. Dulli, S.C. Fehling, C.R. Fisher, S.W. Hodgson, S.W. Keenan, A.N. Kruger, J.W. Mabin, D.L. Mazula, C.A. Monte, A. Olthafer, A.E. Sexton, B.R. Soderholm, A.M. Strom, S. Hati, Comparison of intrinsic dynamics of cytochrome p450 proteins using normal mode analysis, Protein Sci. 24 (2015) 1495–1507, https://doi.org/10.1002/pro.2737.
[28] A. Amadei, M.A. Ceruso, A. Di Nola, On the convergence of the conformational coordinates basis set obtained by the essential dynamics analysis of proteins' molecular dynamics simulations, Proteins Struct. Funct. Bioinforma. 36 (1999)

419–424, https://doi.org/10.1002/(SICI)1097-0134(19990901)36:4<419::AID-PROT5>3.0.CO;2-U.
[29] B. Hess, Convergence of sampling in protein simulations, Phys. Rev. E 65 (2002), https://doi.org/10.1103/PhysRevE.65.031910, 031910.
[30] Cosine Similarity - an Overview, ScienceDirect Topics, (n.d.), https://www.sciencedirect.com/topics/computer-science/cosine-similarity. accessed July 10, 2020.
[31] ProDy: protein dynamics inferred from theory and experiments - PubMed, n.d. https://pubmed.ncbi.nlm.nih.gov/21471012/. accessed July 8, 2020
[32] Y. Wang, M. Liu, J. Gao, Enhanced receptor binding of SARS-CoV-2 through networks of hydrogen-bonding and hydrophobic interactions, Proc. Natl. Acad. Sci. U.S.A. 117 (2020) 13967–13974, https://doi.org/10.1073/pnas.2008209117.
[33] A. Kitao, N. Go, Investigating protein dynamics in collective coordinate space, Curr. Opin. Struct. Biol. 9 (1999) 164–169, https://doi.org/10.1016/S0959-440X(99)80023-2.
[34] Anisotropic network model: systematic evaluation and a new web interface - PubMed, n.d. https://pubmed.ncbi.nlm.nih.gov/16928735/. accessed July 8, 2020
[35] J.A. Jaimes, N.M. André, J.S. Chappie, J.K. Millet, G.R. Whittaker, Phylogenetic analysis and structural modeling of SARS-CoV-2 spike protein reveals an evolutionary distinct and proteolytically sensitive activation loop, J. Mol. Biol. 432 (2020) 3309–3325, https://doi.org/10.1016/j.jmb.2020.04.009.
[36] D. Wrapp, N. Wang, K.S. Corbett, J.A. Goldsmith, C.L. Hsieh, O. Abiona, B.S. Graham, J.S. McLellan, Cryo-EM structure of the 2019-nCoV spike in the prefusion conformation, Science 367 (2020) 1260–1263 (n.d.), https://science.sciencemag.org/content/367/6483/1260. accessed July 21, 2020.